INTERNATIONAL JOURNAL FOR NUMERICAL METHODS IN FLUIDS
Int. J. Numer. Meth. Fluids 2003; **42**:979–997 (DOI: 10.1002/fld.569)

Near-wall turbulence modelling with enhanced dissipation

M. M. Rahman*,† and T. Siikonen

Helsinki University of Technology, Department of Mechanical Engineering, Laboratory of Applied Thermodynamics, Sähkömiehentie 4, FIN-02015 HUT, Finland

SUMMARY

A low-Reynolds number k–ε turbulence model is proposed that incorporates diffusion terms and modified $C_{\tilde{\varepsilon}(1,2)}$ coefficients to amplify the level of dissipation in non-equilibrium flow regions, thus reducing the kinetic energy and length scale magnitudes to improve prediction of adverse pressure gradient flows, involving flow separation and reattachment. Unlike the conventional k–ε model, it requires no wall function/distance parameter that bridges the near-wall integration. The model is validated against a few flow cases, yielding predictions in good agreement with the direct numerical simulation (DNS) and experimental data. Copyright © 2003 John Wiley & Sons, Ltd.

KEY WORDS: wall distance; turbulence; diffusion; flow separation and reattachment

1. INTRODUCTION

Numerous variants of two-equation eddy viscosity models have been devised and often regarded as a favourable compromise between computational accuracy and efficiency to solve fluid flow problems encountered in engineering applications [1–14]. In principle, the high-Reynolds number model is incapable of properly yielding near-wall resolution adhering to wall damping and viscous effects. Abandoning the background of physical and modelling uncertainties, a large number of low-Reynolds number (LRN) modifications have been proposed to two-equation turbulence closures where the integration up to the wall is extremely important. Nonetheless, the modelling of near-wall turbulence in many existing LRN models usually entangles distance to wall as an explicit parameter. This renders the model often inappropriate to simulating complex flows involving multiple surfaces, the wall distance of which becomes cumbersome to define. A remedy to this flaw is to develop a model which implicates no explicit wall distance while integrating it toward the solid surface. The physical rationale behind the LRN model independent of wall topology can be ascribed to Reference [15] ‘matching to wall functions is not trivial, and programming and running time may be reduced by integrating a fixed-up (low-turbulence Reynolds number) model to the wall’.

*Correspondence to: M. M. Rahman, Department of Mechanical Engineering, Helsinki University of Technology, Sähkömiehentie 4, FIN-02015 HUT, Finland.
† E-mail: mizanur.rahman@hut.fi

Received 7 September 2002
Revised 19 February 2003

A wall distance free low-Reynolds number k–ε turbulence closure model is developed. It incorporates the pressure diffusion terms in both the k and ε equations. The model coefficients $C_{\varepsilon(1,2)}$ depend non-linearly on the strain-rate and vorticity invariants. An extra positive source term is embodied with the ε transport equation. Consequently, the model augments the dissipation level in non-equilibrium flow regions, thus reducing the turbulent kinetic energy and length scale magnitudes to improve prediction of adverse pressure gradient flows involving separation and reattachment. The wall singularity is removed by using a physically appropriate time scale that never falls below the Kolmogorov (dissipative eddy) time scale, representing time scale realizability enforcement accompanied by the near-wall turbulent phenomena. An eddy viscosity damping function is designed in terms of the total kinetic energy and invariants of strain-rate and vorticity tensors with no reference to the distance from the wall. In addition, the turbulent Prandtl number σ is adjusted so as to provide substantial turbulent diffusion in the near-wall region. In essence, the model is tensorially invariant, frame-indifferent and applicable to arbitrary topology.

The performance of the new model is demonstrated through the comparison with experimental and DNS data of well documented flows, consisting of fully developed channel flows, a flat plate boundary layer flow with zero pressure gradient, a backward facing step flow, and heat transfer from the circular cylinder in cross flow, respectively.

2. GOVERNING EQUATIONS

The two-dimensional Reynolds-averaged Navier–Stokes (RANS) equations, including the equations for the kinetic energy k and dissipation ε, can be written in the following form:

$$\frac{\partial U}{\partial t} + \frac{\partial (F - F_v)}{\partial x} + \frac{\partial (G - G_v)}{\partial y} = Q \tag{1}$$

where $U = (\rho, \rho u, \rho v, E, \rho k, \rho \varepsilon)^{\mathrm{T}}$. The inviscid fluxes are

$$F = \begin{pmatrix} \rho u \\ \rho u^2 + p + \frac{2}{3}\rho k \\ \rho uv \\ u(E + p + \frac{2}{3}\rho k) \\ \rho uk \\ \rho u\varepsilon \end{pmatrix}, \quad G = \begin{pmatrix} \rho v \\ \rho vu \\ \rho v^2 + p + \frac{2}{3}\rho k \\ v(E + p + \frac{2}{3}\rho k) \\ \rho vk \\ \rho v\varepsilon \end{pmatrix} \tag{2}$$

Here ρ is the density and p is the pressure. The total energy is defined as

$$E = \rho e + \frac{\rho \mathbf{V} \cdot \mathbf{V}}{2} + \rho k \tag{3}$$

where e is the specific internal energy and $\mathbf{V} = u\mathbf{i} + v\mathbf{j}$ is the velocity . The viscous fluxes are

$$F_v = \begin{pmatrix} 0 \\ \tau_{xx} + \frac{2}{3}\rho k \\ \tau_{xy} \\ u\tau_{xx} + v\tau_{xy} - q_x \\ \mu_k(\partial k/\partial x) \\ \mu_\varepsilon(\partial \varepsilon/\partial x) \end{pmatrix}, \quad G_v = \begin{pmatrix} 0 \\ \tau_{xy} \\ \tau_{yy} + \frac{2}{3}\rho k \\ u\tau_{xy} + v\tau_{yy} - q_y \\ \mu_k(\partial k/\partial y) \\ \mu_\varepsilon(\partial \varepsilon/\partial y) \end{pmatrix} \tag{4}$$

and the viscous stress tensor can be given as

$$\tau_{ij} = 2\mu\left(S_{ij} - \frac{1}{3}S_{kk}\delta_{ij}\right) - \rho\overline{u_i u_j} \tag{5}$$

where μ is the laminar viscosity and the Reynolds stresses $\rho\overline{u_i u_j}$ are related to the mean strain-rate tensor S_{ij} through the Boussinesq approximation:

$$-\rho\overline{u_i u_j} = 2\mu_T\left(S_{ij} - \frac{1}{3}S_{kk}\delta_{ij}\right) - \frac{2}{3}\rho k\delta_{ij}, \quad S_{ij} = \frac{1}{2}\left(\frac{\partial u_i}{\partial x_j} + \frac{\partial u_j}{\partial x_i}\right) \tag{6}$$

The heat flux is calculated from

$$\mathbf{q} = -\left(\mu\frac{c_p}{Pr} + \mu_T\frac{c_p}{Pr_T}\right)\nabla T \tag{7}$$

where μ_T is the coefficient of turbulent viscosity, c_p is the specific heat at constant pressure, Pr and Pr_T represent the molecular and turbulent Prandtl numbers, respectively, and T implies the temperature. Clearly, the turbulent part of the total heat flux is estimated using the Boussinesq approximation. The value of Pr_T is chosen to be 0.9 [1]. The diffusion of turbulence is modelled as

$$\mu_k\nabla k = \left(\mu + \frac{\mu_T}{\sigma_k}\right)\nabla k, \quad \mu_\varepsilon\nabla\varepsilon = \left(\mu + \frac{\mu_T}{\sigma_\varepsilon}\right)\nabla\varepsilon \tag{8}$$

where σ_k and σ_ε are the appropriate turbulent Prandtl numbers. The source term Q for the k and ε equations can be written as

$$Q = \begin{pmatrix} \rho P - \rho\varepsilon + \Pi_k \\ \dfrac{C_{\varepsilon 1}\rho P - C_{\varepsilon 2}\rho\varepsilon + E_\varepsilon}{T_t} + \Pi_\varepsilon \end{pmatrix} \tag{9}$$

where the turbulent production term $P = -\overline{u_i u_j}(\partial u_i/\partial x_j)$ and E_ε is a secondary source term designed to increase the level of ε in non-equilibrium flow regions. The symbolized Π_k and Π_ε are the pressure diffusion terms, balancing the molecular diffusion in the near-wall region [2, 3, 16].

3. NEAR-WALL MODELLING

In the vicinity of the wall, the molecular viscosity effect is superior to the turbulent mixing, reflecting a strong anisotropic condition. Consequently, an important criterion regarding the appropriateness of the turbulence model is to represent the near-wall behaviour of turbulence quantities accompanied by a preferential damping of velocity fluctuations in the direction normal to the wall that reconciles the influence of wall proximity adequately.

The realizable time scale T_t included in Eq. (9) can simply be defined as

$$T_t = \sqrt{\frac{k^2}{\varepsilon^2} + C_T^2 \frac{v}{\varepsilon}} = \frac{k}{\varepsilon}\sqrt{1 + \frac{C_T^2}{R_T}}, \quad R_T = \frac{k^2}{v\varepsilon} \tag{10}$$

where v denotes the kinematic viscosity and R_T is the turbulence Reynolds number. Equation (10) warrants that the eddy time scale never falls below the Kolmogorov time scale $C_T\sqrt{v/\varepsilon}$, dominant in the immediate neighbourhood of the solid wall. It prevents the singularity in the dissipation equation down to the wall. Alternatively, the turbulence time scale is k/ε at large R_T but approaches the Kolmogorov limit $C_T\sqrt{v/\varepsilon}$ for $R_T \ll 1$. Nevertheless, the empirical constant C_T associated with the Kolmogorov time scale induces an 'arbitrariness' and the turbulence models constructed so far have deemed values of C_T in the range of 1–6 [4–7]. For the present model, $C_T = \sqrt{2}$ is used which is estimated as follows. In the viscous sublayer $k = y^2/(C_T^2 v/\varepsilon)$, where the basic scale is the Kolmogorov time scale. Besides, the k equation reduces to $v\partial^2 k/\partial y^2 = \varepsilon$ as the wall is approached. Combining these relations provide $C_T = \sqrt{2}$. Obviously, the inclusion of T_t in the ε equation guarantees near-wall asymptotic consistency without resorting to *ad hoc* damping functions employed in many k–ε models [8–10].

To analyse the wall turbulence phenomena, near-wall behaviours of the Reynolds stress $-\overline{uv}$, turbulent kinetic energy k, dissipation rate ε and characteristic time scale T_t are represented around $y = 0$ as [2]

$$k = ay^2 + by^3 + O(y^4) \tag{11}$$

$$\varepsilon = 2va + 4vby + O(y^2) \tag{12}$$

$$\overline{uv} = cy^3 + O(y^4) \tag{13}$$

$$T_t = C_T\sqrt{v/\varepsilon} = y^0/\sqrt{a} + \cdots \tag{14}$$

where the coefficients $a = a(x,z)$, $b = b(x,z)$ and $c = c(x,z)$, given that y is the normal distance from the wall surface.

Since the viscous dissipation presumably dominates near the wall, the eddy viscosity is evaluated from

$$\mu_T = C_\mu f_\mu \rho k T_t \tag{15}$$

where $C_\mu = 0.09$ and the dynamic time scale k/ε is replaced by T_t, a distinct turbulence time scale. The damping function is chosen pragmatically as

$$f_\mu = f_\lambda \left(1 + \frac{25}{R_\lambda^2}\right)\sqrt{\frac{\sigma_\varepsilon}{\sigma_k}}, \quad R_\lambda = \sqrt{\frac{K_T}{\nu\eta}}$$

$$f_\lambda = \tanh(C_1 R_\lambda + C_2 R_\lambda^2), \quad K_T = \mathbf{V}\cdot\mathbf{V}/2 + k \tag{16}$$

where $C_1 = 3\times10^{-3}$ and $C_2 = 4\times10^{-4}$. The parameter $\eta = \max(S, W)$, containing the invariants of strain-rate and vorticity respectively; $S = \sqrt{2S_{ij}S_{ij}}$ and $W = \sqrt{2W_{ij}W_{ij}}$. The mean vorticity tensor W_{ij} is defined as

$$W_{ij} = \frac{1}{2}\left(\frac{\partial u_i}{\partial x_j} - \frac{\partial u_j}{\partial x_i}\right) \tag{17}$$

The coefficient $\sqrt{\sigma}$-ratio associated with f_μ is modelled subsequently, rather than being assigned a value (unlike the commonly adopted practice with $\sigma_k = 1.0$, and $\sigma_\varepsilon = 1.3$).

The empirical function f_μ is valid in the whole flow field, including the viscous sublayer and the logarithmic layer. In the region close to the wall, the Reynolds stress $-\overline{uv} \sim y^3$ and $k \sim y^2$. To preserve the correct cubic power-law behaviour of $-\overline{uv}$, the damping function needs to increase proportionally to y^{-1} in the near-wall region. Equation (16) confirms that as $y \to 0$, $R_\lambda \sim y$ and hence $f_\mu \sim y^{-1}$. Alternatively, the adopted form of f_μ reproduces correctly the asymptotic limit, involving the distinct effects of low-Reynolds number and wall proximity. As evinced by Figure 1 in comparison with the DNS data [16] for fully developed turbulent channel flows, the proposed function $f_\mu = 1$ remote from the wall to ensure the model being compatible to the standard k–ε turbulence model. The use of R_λ (a new parameter with no reference to the distance from the solid surface) confronts the singularity at neither the separating nor the reattaching point in contrast to the adoption of $y^+ = u_\tau y/\nu$, where u_τ is the friction velocity. Consequently, the model is applicable to separated and reattaching flows. In principle, the eddy viscosity envisages two separate effects, comprising the influences of low-Reynolds number and wall proximity.

The budgets of k and ε from the DNS data approve that the role of turbulent diffusion in the near-wall region is substantial. Accordingly, the values of Prandtl number σ_k and σ_ε are formulated as

$$\sigma_k = \frac{C_{\varepsilon 2}}{C_{\varepsilon 1}}[\sqrt{C_\nu}(C_{\varepsilon 2} - C_{\varepsilon 1}) + f_\sigma], \quad \sigma_\varepsilon = \frac{\sigma_k}{1.1}(1 - C_\nu f_\sigma)^{-1} \tag{18}$$

where $f_\sigma = 3f_\lambda/(1 + 2f_\lambda^2)$. The distribution of σ is depicted in Figure 1. The quantities $C_{\varepsilon(1,2)}$ and C_ν are determined later. The model coefficients σ_k and σ_ε are developed such that sufficient diffusion is obtained in the vicinity of the wall and in the core region of the flow $\sigma_k/\sigma_\varepsilon = 1$ to eliminate the common drawback where the turbulent diffusion of k overwhelms the diffusion of ε with $\sigma_k < \sigma_\varepsilon$. To this end, it must be stressed that the modification to f_μ (rather than excluding $\sqrt{\sigma}$-ratio traditionally) in Equation (16) reduces the potentiality of f_μ to grow particularly in near-wall regions as represented faithfully by Figure 1, thereby facilitating avoidance of excessive eddy viscosity.

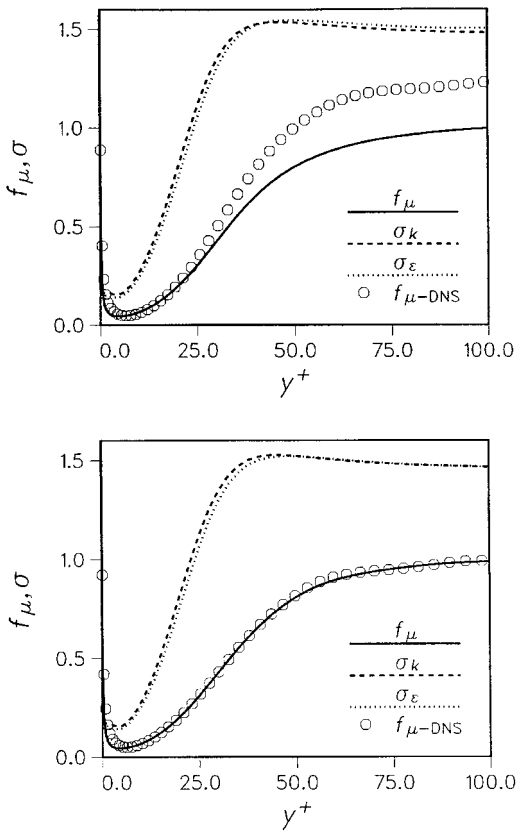

Figure 1. Variations of f_μ and σ with wall distance in channel flow: (a) $Re_\tau = 180$ and (b) $Re_\tau = 395$.

Near-wall flows show a tendency to underestimate the dissipation rate ε due to the local anisotropy of turbulence, adhering to the non-dimensional parameter P/ε [11, 17]. The formulation has been developed to enhance dissipation in such situation using the relation: $C_{\varepsilon 1} = C^*_{\varepsilon 1}(a_1 + a_2 P/\varepsilon)$, where $C^*_{\varepsilon 1}$, a_1 and a_2 are model constants [12, 13]. However, this procedure can cause numerical instability in more complex flows. One possible approach to counteracting this adverse situation is to explore alternative elements with relevance to P/ε:

$$\begin{aligned} C_{\varepsilon 1} &= 1 + 1.35\sqrt{C_v \frac{P}{\varepsilon}}, \quad C_{\varepsilon 2} = 1.4\left(1 + \sqrt{C_v \frac{P}{\varepsilon}}\right) \\ \frac{P}{\varepsilon} &= C_v T_t^2 \eta^2, \quad C_v = \frac{1}{2(1 + T_t\sqrt{S^2 + W^2})} \end{aligned} \tag{19}$$

It is appropriate to emphasize herein that the proposed relation meets the requirement of the equilibrium state $P/\varepsilon \approx 1$ for the logarithmic region in a turbulent channel flow, where $T_t S = T_t W \approx 3.3$ [7]. Remarkably, the average $C_{\varepsilon 2}/C_{\varepsilon 1} = 1.3$ for the channel flow, converging toward the standard $C_{\varepsilon 2}$-to-$C_{\varepsilon 1}$ ratio ($1.92/1.44 \approx 1.33$). As approved by Figure 2, the rational

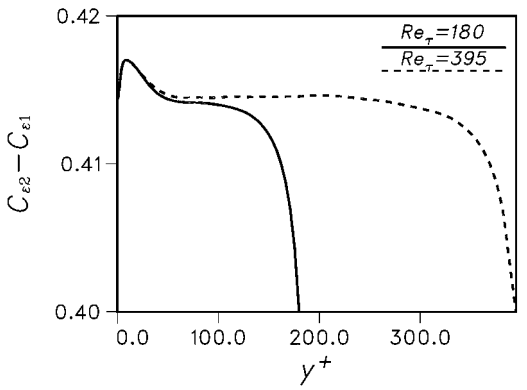

Figure 2. Distribution of $C_{\varepsilon 2} - C_{\varepsilon 1}$ with wall distance in channel flow.

subsistence (T_t, S, W) to P/ε indubitably is conducive to allowing compatible changes in both $C_{\varepsilon 1}$ and $C_{\varepsilon 2}$ that account for the additional production of dissipation by the anisotropy of turbulence.

The extra source term E_ε in Equation (9) is constructed from the most extensive turbulent diffusion models for k and ε equations derived by Yoshizawa [18] with the two-scale direct-interaction approach using the inertial-range simplification. To receive positive benefits from the numerical reliability and to integrate the inertial-range condition directly to the solid wall, the cross-diffusion term is designed with an assistance of Reference [14] as

$$E_\varepsilon = C_\varepsilon \frac{\mu_T}{T_t} \max\left[\frac{\partial(k/\varepsilon)}{\partial x_j}\frac{\partial k}{\partial x_j}, 0\right], \quad C_\varepsilon = \sqrt{C_{\varepsilon 1}^2 + C_{\varepsilon 2}^2} \tag{20}$$

Obviously, the source term E_ε stimulates the energy dissipation in non-equilibrium flows, thereby reducing the departure of the turbulent length scale from its local equilibrium value and enabling improved prediction of adverse pressure gradient flows accompanied by flow separation and reattachment. At this stage, it appears necessary to identify that the quantity E_ε is characteristically beneficial in the vicinity of reattachment point and hence, it can be regarded as an attempt at replacing the Yap correction [19].

In the vicinity of the wall, convection, turbulent diffusion and production approach zero very rapidly. Consequently, the k equation in the near-wall region can be deduced as

$$\nu\frac{\partial^2 k}{\partial y^2} - \varepsilon + \frac{\Pi_k}{\rho} = 0 \tag{21}$$

With Equations (11) and (12), the expansion relation from Equation (21) is obtained as

$$\frac{\Pi_k}{\rho} + 2\nu b y + O(y^2) = 0 \tag{22}$$

necessitating that Π_k/ρ must have the near-wall behaviour $-2\nu b y$ to balance the k equation in the vicinity of the solid surface. Subsequently, near the wall the asymptotic behaviour of

the remaining terms in the ε equation can deliberately be derived as

$$\nu\frac{\partial^2\varepsilon}{\partial y^2}\sim y^0,\quad \frac{C_{\varepsilon 2}\varepsilon}{T_t}\sim y^0 \tag{23}$$

indicating that Π_ε must possess the wall limiting behaviour $\Pi_\varepsilon\sim y^0$, having agreement with the DNS. In addition, DNS manifests that the influences of pressure diffusion terms decay quickly away from the wall. To preserve the above-mentioned requirements appropriately, the pressure diffusion terms Π_k and Π_ε are modelled as follows:

$$\Pi_k=-\frac{\partial}{\partial x_j}\left(C_v\frac{\mu k}{\varepsilon}\frac{\partial\varepsilon}{\partial x_j}\right),\quad \Pi_\varepsilon=-\frac{\partial}{\partial x_j}\left(C_v\frac{\mu}{T_t}\frac{\partial k}{\partial x_j}\right) \tag{24}$$

where $C_v\approx\frac{1}{2}$ at the wall as estimated with reference to Equations (10) and (19). A close look at the entire contrivance and to the DNS data for channel flow, reveals that a value of $\frac{1}{2}$ associated particularly with the modelled Π_ε is prone to avoid imbalance between the molecular diffusion and Π_ε at the wall, compromising inherently with the limit of near-wall balance in the ε equation. Since $C_v=C_v(T_t,S,W)$, Π must loose its influence outside the close proximity of the wall due to natural damping. Essentially, the compatibility relation (24) mimics the diffusive nature of the pressure diffusion, resembling the conventional cross-diffusion model [18]. The content within the brackets can be analogized to that employed in Equation (8) and computed accordingly.

The transport equations for k and ε are subjected to the following boundary conditions at solid walls:

$$k_w=0,\quad \varepsilon_w=2\nu\left(\frac{\partial\sqrt{k}}{\partial y}\right)^2\approx 2\nu\frac{k}{y_n^2} \tag{25}$$

To avoid numerical instability, the approximation for ε_w is applied at the first grid node neighbouring the wall, rather than on the wall itself. This requires normal distance from a wall to the nearest grid point, which is unambiguous and readily available. The validity of Equation (25) necessitates that the grid system is fine enough to produce the near-wall limiting behaviour.

4. COMPUTATIONS

To ascertain the efficacy of the proposed model, a few applications to two-dimensional turbulent flows consisting of a fully developed channel flow, a flat plate boundary layer flow with zero pressure gradient, a backward facing step flow, and heat transfer from a circular cylinder in cross flow are considered. For a comparison purpose, calculations from the original Chien (OCH) model [10] and the modified Chien (MCH) model [14] are included. A cell centred finite-volume scheme combined with an artificial compressibility approach is employed to solve the flow equations [20, 21]. A fully upwinded second-order spatial differencing is applied to approximate the convective terms. Roe's [22] damping term is used to calculate the flux on the cell face. A diagonally dominant alternating direction implicit (DDADI) time integration method [23] is applied for the iterative solution to the discretized

equations. A multigrid method is utilized for the acceleration of convergence [24]. The basic implementation of the artificial compressibility method and associated features are described in References [20, 21, 25].

4.1. Channel flow

Computations are carried out for fully developed turbulent channel flows at $Re_\tau = 180$ and 395, for which turbulence quantities are attainable from the DNS data [16]. Calculations are conducted in the half-width of the channel, imposing periodic boundary conditions, except for the pressure, pertaining to the upstream and downstream boundaries. Computations involving a 48×32 non-uniform grid refinement for $Re_\tau = 180$ and 48×48 for $Re_\tau = 395$ are considered to be sufficiently accurate to describe the flow characteristics. For both cases, the length of the computational domain is 32δ, where δ is the channel half-width. To ensure the resolution of viscous sublayer the first grid node near the wall is placed at $y^+ \approx 0.4$. Comparisons are made by plotting the results in the form of $u^+ = u/u_\tau$, $k^+ = k^+/u_\tau^2$, $\overline{uv}^+ = \overline{uv}/u_\tau^2$ and $\varepsilon^+ = v\varepsilon/u_\tau^4$ versus y^+.

Figure 3 shows the velocity profiles for different models. Predictions of both the present and MCH models agree well with the DNS data. The OCH model slightly overestimates the

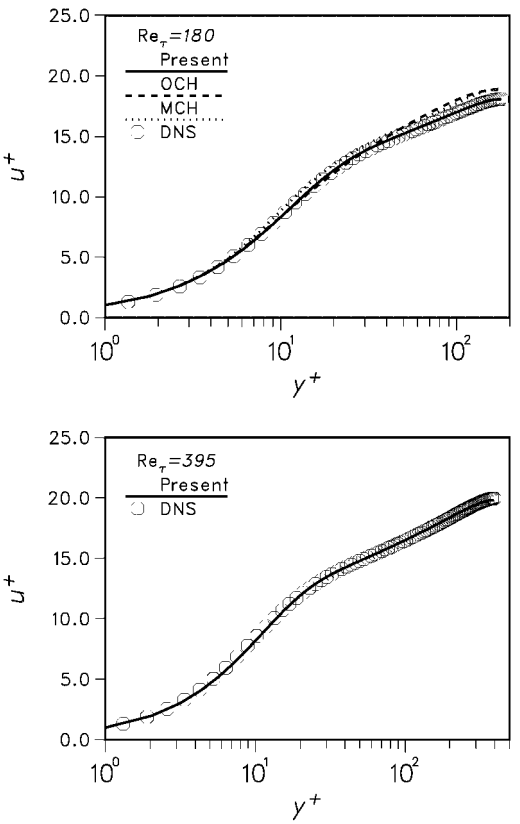

Figure 3. Mean velocity profiles of channel flow.

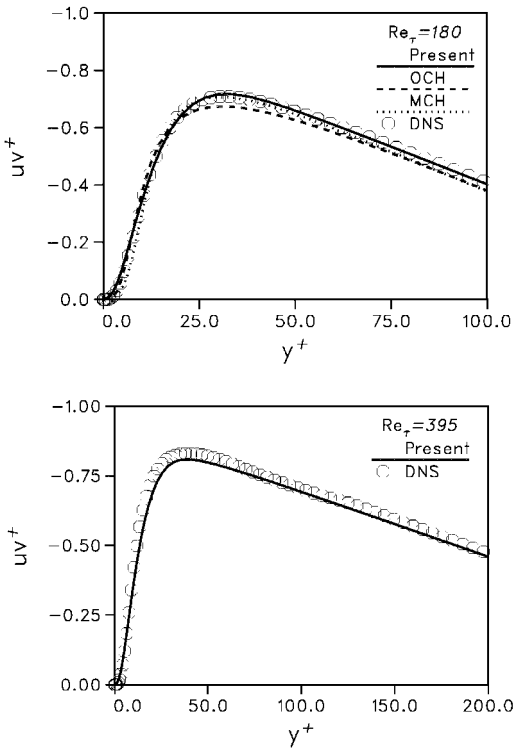

Figure 4. Shear stress profiles of channel flow.

mean velocity profile in the outer layer. Profiles of turbulent shear stresses are displayed in Figure 4. Agreement of all model predictions with the DNS data seems to be almost perfect.

Further examination of the model performances can be directed to the k^+ profiles as portrayed in Figure 5 for the near-wall region. As is evident, the present model prediction is in broad accord with the MCH model and DNS data. On the contrary, the OCH model predicts a peak at a slightly shifted location. Figure 6 exhibits the profiles of ε^+ from the three computations. The present model provides a maximum ε^+ at the wall which is more in line with the experimental and DNS data. In strong contrast, the OCH and MCH models indicate misplaced local maxima.

4.2. Flat plate boundary layer flow

The performance of the proposed model is further contrasted with the experimental data of the flow over a flat plate with a high free stream turbulence intensity. The test case is taken from 'ERCOFTAC' Fluid Dynamics Database WWW Services (http://fluindigo. mech.surrey.ac.uk/) preserved by P. Voke. Measurements down to $x = 1.495$ m which corresponds to $Re_x \approx 94\,000$, are made by J. Coupland at Rolls-Royce. The inlet velocity is 9.4 m/s and the pressure

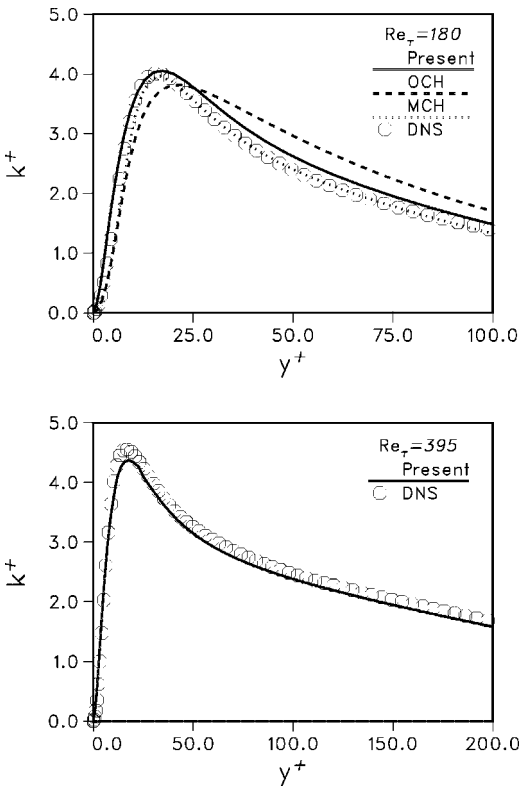

Figure 5. Turbulence kinetic energy profiles of channel flow.

gradient is zero. The upstream turbulence intensity $\mathrm{Tu} = 6.0\%$, defined as $\mathrm{Tu} = \sqrt{\frac{2}{3}k}/U_{\mathrm{ref}}$, where U_{ref} indicates the reference velocity. The dissipation is set so that the decay of free stream turbulence is in balance.

Computations begin 16 cm ahead of the leading edge and symmetric conditions are applied. The length and height of the grid are 1.6 and 0.3 m, respectively. The near-wall grid node is located at $y^+ < 1.0$, except the point at the leading edge ($y^+ = 2.1$). The grid size is 96×64 and heavily clustered near the wall.

The predicted skin friction coefficients ($C_f = 2u_\tau^2/U_{\mathrm{ref}}^2$) are compared with the experimental data in Figure 7. The overall performance in predicting the friction coefficient is the best for the present model, exhibiting an interesting feature that the transition starts at the right position and it is strong enough. In contrast, both the OCH and MCH models, having the wall distance in the damping functions provide earlier transition than that seen in the experiment, coincident with Savill's investigation [26]. Seemingly, the agreement between the computations and the experiment is fairly good toward the end of the transition (e.g. beyond $x = 0.195\,\mathrm{m}$). However, the MCH model prediction is somewhat on a lower level than the data show.

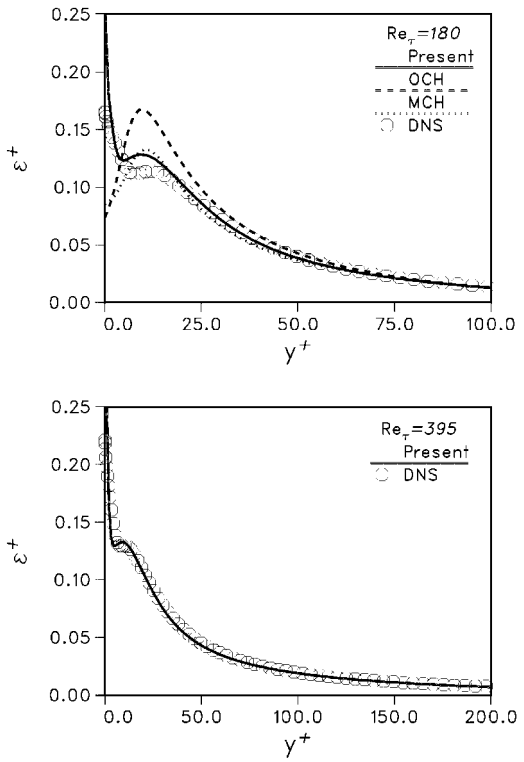

Figure 6. Dissipation rate profiles of channel flow.

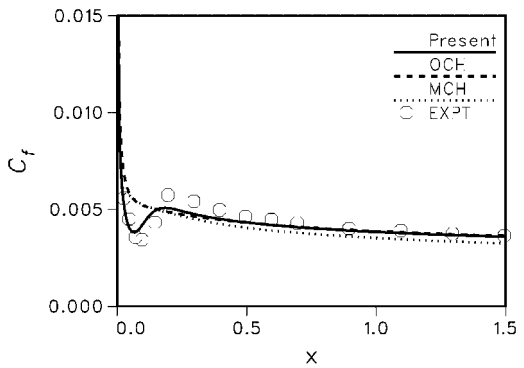

Figure 7. Streamwise skin-friction coefficient of boundary layer flow.

4.3. Backward facing step flow

To validate the performance in complex separated and reattaching turbulent flows, the present model is applied to the flow over a backward facing step. The computations are conducted

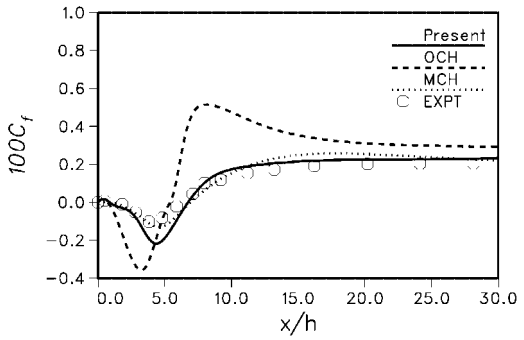

Figure 8. Skin-friction coefficient along the step-side bottom wall.

corresponding to the experimental case with zero deflection of the wall opposite to the step, as investigated by Driver and Seegmiller [27]. The reference velocity $U_{\text{ref}} = 44.2\,\text{m/s}$ and the step height $h = 0.0127\,\text{m}$. The ratio between the channel height and the step height is 9, and the step height Reynolds number is $Re = 37\,500$. At the channel inlet, the Reynolds number based on the momentum thickness is $Re_\theta = 5000$.

For the computations, grids are arranged in two blocks. The smaller one (extended from the inlet to the step) contains a 16×48 non-uniform grid and the grid size for other one is 120×80. The inlet conditions are specified four step heights upstream of the step corner and the outlet boundary conditions are imposed 30 step heights downstream of the step corner. The inlet profiles for all dependent variables are generated by solving the models at the appropriate momentum thickness Reynolds number. All the quantities shown below are normalized by the step height h and the experimental reference free stream velocity U_{ref}, provided that the distance x/h is measured exactly from the step corner.

Computed and experimental friction coefficients C_f along the bottom wall (step side wall) are plotted in Figure 8. As is observed, the OCH model gives the C_f distribution with a large overshoot followed by a sudden drop in the immediate vicinity of the reattachment point. Apparently, the ambiguous prediction regarding the OCH model is attributable to shortcomings in the y^+ dependence viscous damping functions employed. The MCH and present models predict the skin friction coefficient qualitatively. The positive C_f that starts from $x/h = 0$, is due to a secondary eddy which sits in the corner at the base of the step, inside the main recirculation region. The recirculation length predicted by each model can be determined by measuring the distance from the step corner to a point at which the curve changes sign. The OCH model predicts a recirculation length of 5.4, and the corresponding predictions by the MCH and present models are 6.8 and 6.6. The experimental value of the reattachment length is 6.26 ± 0.1, making a fairly good correspondence with the MCH and present models.

The streamwise mean velocity profiles at four representative positions are depicted in Figure 9. Obviously, the predictions of all models are in good agreement with the experiment. It is a bit nebulous that the inaccurate prediction of the C_f distribution by the OCH model has little effect on the velocity profiles.

Comparisons are extended to the distributions of the turbulent kinetic energy and the corresponding Reynolds shear stress at different x/h locations behind the step corner, as shown

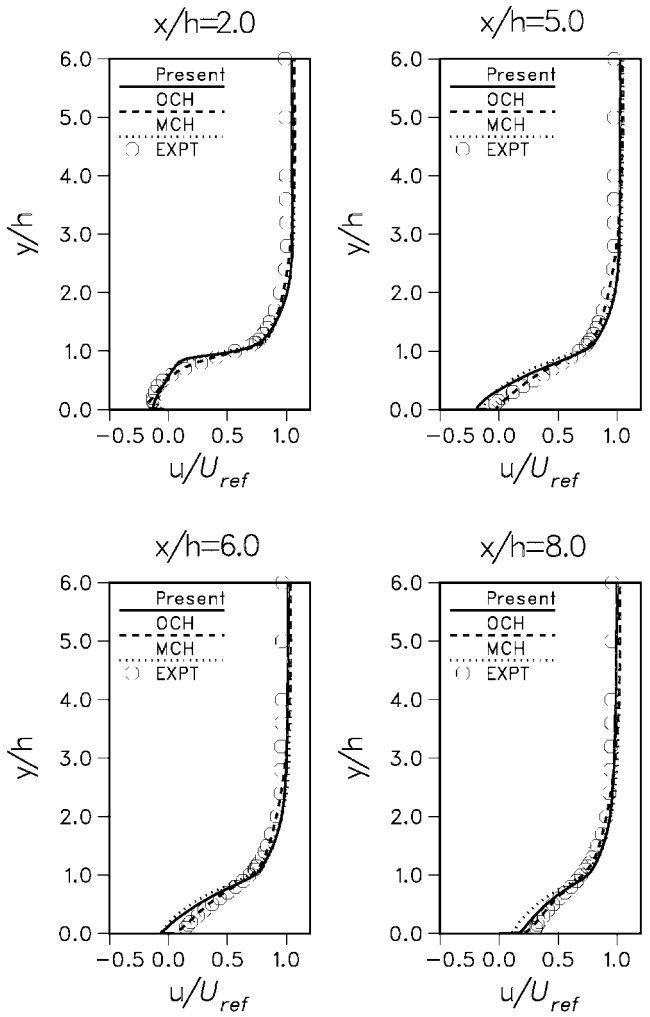

Figure 9. Mean velocity profiles at selected locations for step flow.

in Figures 10 and 11. Since the $\overline{ww}$ component is not measured in the experiment, the usual approximation $k \approx 3/4(\overline{uu} + \overline{vv})$ is employed. A closer inspection of the distribution indicates that the present model predictions are in a broad agreement with the experimental data. On average, the agreement is good in both the recirculation and recovery regions.

4.4. Heat transfer from circular cylinder in cross flow

The performance of the proposed model is further evaluated by comparing with the experimental data of turbulent heat transfer around a circular cylinder at $Re = 3.6 \times 10^4$ in cross flow [28]. Probably, this is a typical Re for practical heat exchangers. The configuration is geometrically simple but difficult to model. The reasoning is most likely to be attributed to

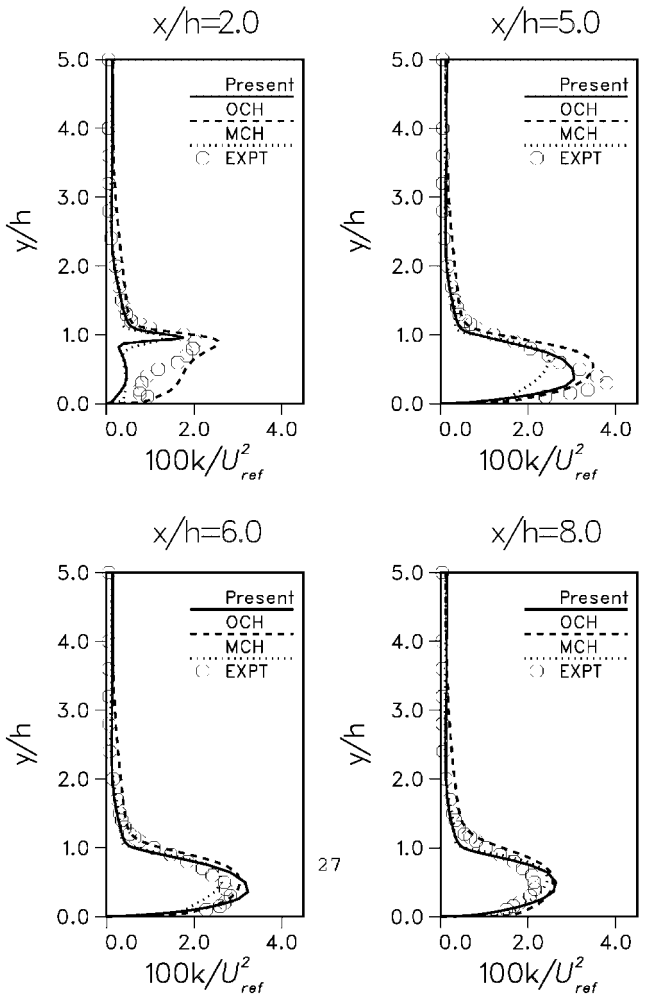

Figure 10. Kinetic energy profiles at selected locations for step flow.

the boundary layer separation, leading to another complex environment. The tested cylinder consists of a tube with $D = 0.025$ m, where D is the diameter. The reference velocity is $U_{\text{ref}} = 22.85$ m/s with an upstream turbulence intensity $\text{Tu} = 0.5\%$. An O type grid with 128×96 resolution, clustered heavily near the solid wall, is employed. The radial length of the computational domain is $60D$. External boundary, that is, far field, conditions are applied. A constant temperature is prescribed at the wall, which simulates the experimental boundary conditions.

Figure 12 portrays the variation of the local Nusselt number with the azimuth angle. As can be seen, the distribution exhibits the characteristic feature of a minimum Nusselt number at the separation that corresponds to $\theta \approx 85°$, followed by an increase in heat transfer in the wake regions. Obviously, the present model prediction maintains good agreement with the experiment.

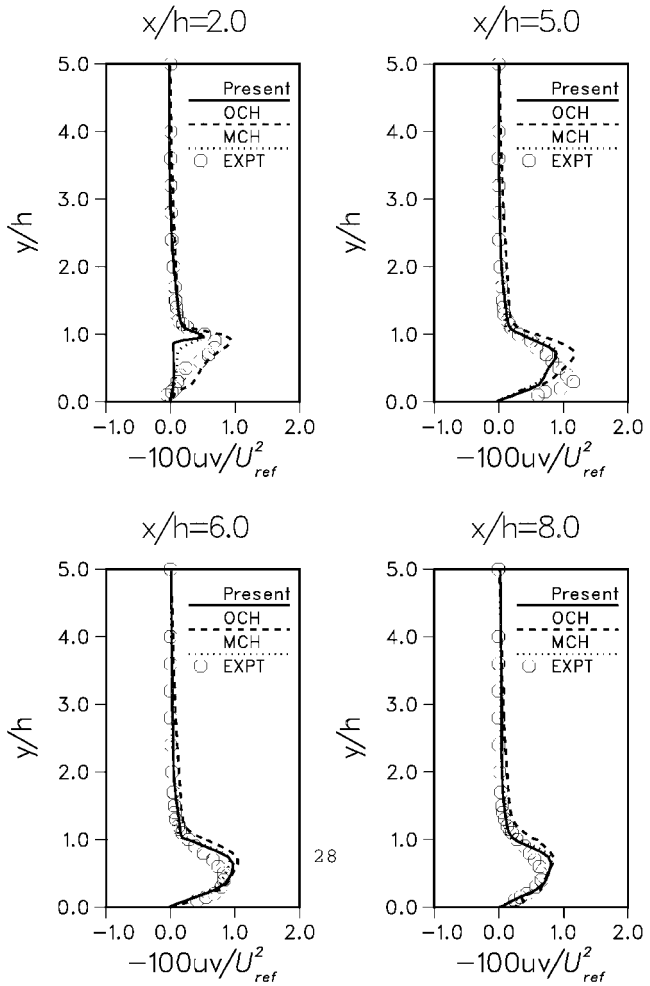

Figure 11. Shear stress profiles at selected locations for step flow.

5. CONCLUSIONS

The proposed turbulent model is wall distance free, tensorially invariant and frame-indifferent. Consequently, it is applicable to arbitrary topology in conjunction with structured or unstructured grids. The model is susceptible to the near-wall and low-Reynolds number effects emanating from the physical requirements. The potential importance of the damping functions is conspicuous. The anisotropic production in the dissipation equation is accounted for substantially by modifying the model constants $C_{\varepsilon(1,2)}$ and adding a secondary source term, leading to a reduced level of turbulence generation in non-equilibrium flow regions. Consequently, the model is capable of evaluating the flow cases entangling separation and reattachment. Contrasting the predicted results with measurements demonstrates that the

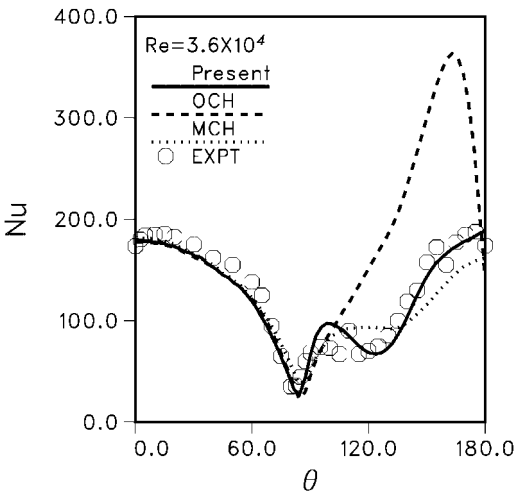

Figure 12. Local Nusselt number distribution over half of tube surface.

present model reproduces correctly the skin-friction coefficients and the near-wall heat transfer behaviour.

NOMENCLATURE

C_f	friction coefficient
C_μ	eddy viscosity coefficient
D	diameter of a round tube
e	specific internal energy
E	total internal energy
f_μ	viscous damping function
F, G	flux vectors in x, y directions
h	step height
k	turbulent kinetic energy
Nu	local Nusselt number
p	static pressure
P	turbulent production term
Pr	Prandtl number
q	heat flux
Q	source term
S	mean strain-rate invariant
t	time
T_t	realizable time scale
u, v	velocity components in x, y directions
$-\rho\overline{u_i u_j}$	Reynolds stresses

W	mean vorticity invariant
x, y	Cartesian coordinates
y^+	non-dimensional normal distance from wall

Greek letters

δ	half-width of a channel
δ_{ij}	Kronecker's delta
ε	turbulent dissipation
μ, μ_T	laminar and eddy viscosities
ν	molecular kinematic viscosity
ρ	density
σ	turbulent Prandtl number

Subscripts

T	turbulent condition
ref	reference condition
v	viscous part

REFERENCES

1. Jones WP, Launder BE. The calculation of low-Reynolds number phenomena with a two-equation model of turbulence. *International Journal of Heat and Mass Transfer* 1973; **16**:1119–1130.
2. Hwang CB, Lin CA. Improved low-Reynolds number k–$\tilde{\varepsilon}$ model based on direct numerical simulation data. *AIAA Journal* 1998; **36**:38–43.
3. Nagano Y, Kondoh M, Shimada M. Multiple time scale turbulence model for wall and homogeneous flows based on direct numerical simulations. *International Journal of Heat and Fluid Flow* 1997; **18**:346–359.
4. Durbin PA. Near-wall turbulence closure modelling without damping functions. *Theoretical Computational Fluid Dynamics* 1991; **3**:1–13.
5. Goldberg U, Apsley D. A wall-distance-free low RE k–ε turbulence model. *Computer Methods in Applied Mechanics and Engineering* 1997; **145**:227–238.
6. Yang Z, Shih TH. New time scale based k–ε model for near-wall turbulence. *AIAA Journal* 1991; **29**: 1337– 1340.
7. Rahman MM, Rautaheimo P, Siikonen T. Modifications for an explicit algebraic stress model. *International Journal for Numerical Methods in Fluids* 2001; **35**:221–245.
8. Henjalic K, Launder BE. Contribution towards a Reynolds-stress closure for low-Reynolds number turbulence. *Journal of Fluid Mechanics* 1976; **74**:593–610.
9. Nagano T, Tagawa M. An improved $k-\varepsilon$ model for boundary layer flows. *Journal of Fluids Engineering* 1990; **112**:33–39.
10. Chien K-Y. Predictions of channel and boundary layer flows with a low-Reynolds number turbulence model. *AIAA Journal* 1982; **20**:33–38.
11. Mansour NN, Kim J, Moin P. Near-wall k–ε turbulence modeling. *AIAA Journal* 1989; **27**:1068–1073.
12. Durbin PA. A Reynolds-stress model for near-wall turbulence. *Journal of Fluid Mechanics* 1993; **249**:465–498.
13. Ahn JW, Park TS, Sung HJ. Application of a near-wall turbulence model to the flows over a step with inclined wall. *International Journal of Heat and Fluid Flow* 1997; **18**:209–217.
14. Rahman MM, Siikonen T. Improved low-Reynolds-number k–$\tilde{\varepsilon}$ model. *AIAA Journal* 2000; **38**:1298–1300.
15. Bradshaw P. Turbulence modeling with application to turbo-machinery. *Progress in Aerospace Science* 1996; **32**:575–624.
16. Mansour NN, Kim J, Moin P. Reynolds-stress and dissipation-rate budgets in a turbulent channel flow. *Journal of Fluid Mechanics* 1988; **194**:15–44.
17. Durbin PA, Speziale CG. Local anisotropy in strained at high Reynolds numbers. *Journal of Fluids Engineering* 1991; **113**:707–709.
18. Yoshizawa A. Statistical modeling of a transport equation for the kinetic energy dissipation rate. *Physics of Fluids A* 1987; **30**:628–631.

19. Yap CR. Turbulent heat and momentum transfer in recirculating and impinging flows. *Ph.D. thesis*, Faculty of Technology, University of Manchester, 1987.
20. Rahman MM, Rautaheimo P, Siikonen T. Numerical study of turbulent heat transfer from a confined impinging jet using a pseudo-compressibility method. In *Second International Symposium on Turbulence, Heat and Mass transfer*, Delft, The Netherlands, Hanjalic K, Peeters TWJ (eds). Delft University Press: Delft, 1997; 511–520.
21. Rahman MM, Siikonen T. An artificial compressibility method for incompressible flows. *Numerical Heat Transfer, Part B* 2001; **40**:391–409.
22. Roe PL. Approximate Riemann solvers, parameter vectors, and difference Schemes. *Journal of Computational Physics* 1981; **43**:357–372.
23. Lombard C, Bardina J, Venkatapathy E, Oliger J. Multi-dimensional formulation of CSCM—an upwind flux difference eigenvector split method for the compressible Navier–Stokes equations. In *Sixth AIAA Computational Fluid Dynamics Conference*, AIAA Paper 83-1895-CP, 1983; 649–664.
24. Jameson A, Yoon S. Multigrid solution of the Euler equations using implicit schemes. *AIAA Journal* 1986; **24**:1737–1743.
25. T. Siikonen, An application of Roe's flux-difference splitting for k–ε turbulence model. *International Journal for Numerical Methods in Fluids* 1995; **21**:1017–1039.
26. Savill AM. Some recent progress in the turbulence modeling of by-pass transition. In *Near-Wall Turbulent Flows*, So RMC, Speziale CG, Launder BE (eds). Elsevier: 1993; 829–848.
27. Driver DM, Seegmiller HL. Features of a reattaching turbulent shear layer in divergent channel flow. *AIAA Journal* 1985; **23**:163–171.
28. Scholten JW, Murray DB. Unsteady heat transfer and velocity of a cylinder in cross flow—I. low free stream turbulence. *International Journal of Heat and Mass Transfer* 1998; **41**:1139–1148.

